C-Terminal Half of Human Centrin 2 Behaves like a Regulatory EF-Hand Domain†

Elena Matei,‡ Simona Miron,‡ Yves Blouquit,‡ Patricia Duchambon,‡ Isabelle Durussel,§ Jos A. Cox,§ and Constantin T. Craescu*,‡

INSERM U350 and Institut Curie-Recherche, Centre Universitaire, Bâtiments 110-112, 91405 Orsay, France, and Département de Biochimie, Université de Genève, 1211 Genève, Switzerland

Received October 8, 2002; Revised Manuscript Received December 19, 2002

ABSTRACT: Human centrin 2 (HsCen2) is an EF-hand protein that plays a critical role in the centrosome duplication and separation during cell division. We studied the structural and Ca^{2+}-binding properties of two C-terminal fragments of this protein: SC-HsCen2 (T94-Y172), covering two EF-hands, and LC-HsCen2 (M84-Y172), having 10 additional residues. Both fragments are highly disordered in the apo state but become better structured (although not conformationally homogeneous) in the presence of Ca^{2+} and depending on the nature of the cations (K^+ or Na^+) in the buffer. Only the longer C-terminal domain, in the Ca^{2+}-saturated state and in the presence of Na^+ ions, was amenable to structure determination by nuclear magnetic resonance. The solution structure of LC-HsCen2 reveals an open two EF-hand structure, similar to the conformation of related Ca^{2+}-saturated regulatory domains. Unexpectedly, the N-terminal helix segment (F86-T94) lies over the exposed hydrophobic cavity. This unusual intramolecular interaction increases considerably the Ca^{2+} affinity and constitutes a useful model for the target binding.

The microtubule organizing centers (MTOC) are cytoplasmic organelles, encountered in almost all the eukaryotic cells having an important role in the nucleation of the microtubules and the regulation of their dynamics. Before the mitosis, the MTOC duplicates and the two resulting organelles define the two poles of the mitotic spindle. In a later phase, the microtubule attachment to the chromosomes permits equal segregation of the genetic material. Alteration of the MTOC duplication could perturb severely the bipolar spindle formation, and this blocks the cell in the G2/M phase. In contrast, hyper amplification of the centrosome is associated with cellular transformation and cancer (*1*, *2*).

The animal MTOC, called the centrosome, is about 1 μ^3 and consists of two short cylindrical centrioles, usually oriented perpendicular to each other, and a pericentriolar material that contains about 100 proteins (*3*). One of them, centrin, is a ubiquitous, highly conserved protein in diverse evolutionary lineages, including algal, higher plant, invertebrate, and mammalian cells (*4*). It is an acidic protein of 19.5 kDa belonging to the highly conserved EF-hand calmodulin (CaM)[1] super family of Ca^{2+}-binding proteins. Comparative sequence analysis suggests that centrins have two structural domains, each containing two EF-hand motifs. In humans, there are at least three centrin isoforms (*5*−*7*) with variable sequences. HsCen1 and HsCen2 (84% sequence identity) may play a role in centrosome segregation or cytokinesis. About 10% of HsCen2 is found in nuclear fractions, and this dual localization was thought to reflect its capacity to coordinate the nuclear and cytoplasmic division processes (*8*). HsCen3 is the closest human homologue of yeast Cdc31 (59% sequence identity) and appears to play a role in centrosomal duplication (*9*). Analysis of the cell ultrastructure and studies on centrin aggregation (*10*) lead to the proposal that centrins may control the morphology and dynamics of the cell cycle machinery (*11*). Thus, the available data indicate that human centrins have the capacity to accomplish multiple cellular functions.

Despite an increasing amount of experimental results indicating the critical role played by human centrins in the centrosome-controlled cellular division, the molecular and physicochemical basis of their functions is still poorly characterized. Among the related centrins, that of *Chlamydomonas reinhardtii* algae was the subject of more detailed biophysical studies (*12*−*14*). Investigation of the global structural and functional properties, using CD, FTIR, and NMR spectroscopy, showed that the two domains of this protein have a structural autonomy and bind Ca^{2+} or a target peptide (from the yeast Kar1 protein) independently of each other (*13*). Both N- and C-terminal halves exhibit significant Ca^{2+} affinity and undergo metal-induced conformational changes, which may have a physiological relevance. Despite a high sequence identity (71%) between *Chlamydomonas* centrin and HsCen2, the human variant, studied in standard conditions (Tris-HCl buffer and 150 mM KCl), showed only one high affinity Ca^{2+} binding site per molecule, most probably in the C-terminal domain (*15*). Understanding of this sequence dependent functional difference, and more generally, of the specific functional properties of the various

† Supported by the Institut Curie, the Institut National de la Santé et de la Recherche Médicale, the Centre National de la Recherche Scientifique, and the Swiss National Science Foundation. S.M. is a recipient of a Marie Curie fellowship from European Community.

* Corresponding author. Tel.: 33 1 69 86 31 63. Fax: 33 1 69 07 53 27. E-mail: Gil.Craescu@curie.u-psud.fr.

‡ INSERM U350 and Institut Curie.

§ Université de Genève.

[1] Abbreviations: CaM, calmodulin; HsCen2, human centrin 2; SC-HsCen2, short C-terminal fragment of human centrin2 (T94-Y172); LC-HsCen2, longer C-terminal fragment of human centrin 2 (M84-Y172); TnC, troponin C; TCA, trichloroacetic acid; TNS, 2-*p*-toluidinylnaphthalene-6-sulfonate; PAGE, polyacrylamide gel electrophoresis.

10.1021/bi0269714 CCC: $25.00
Published on Web 01/25/2003

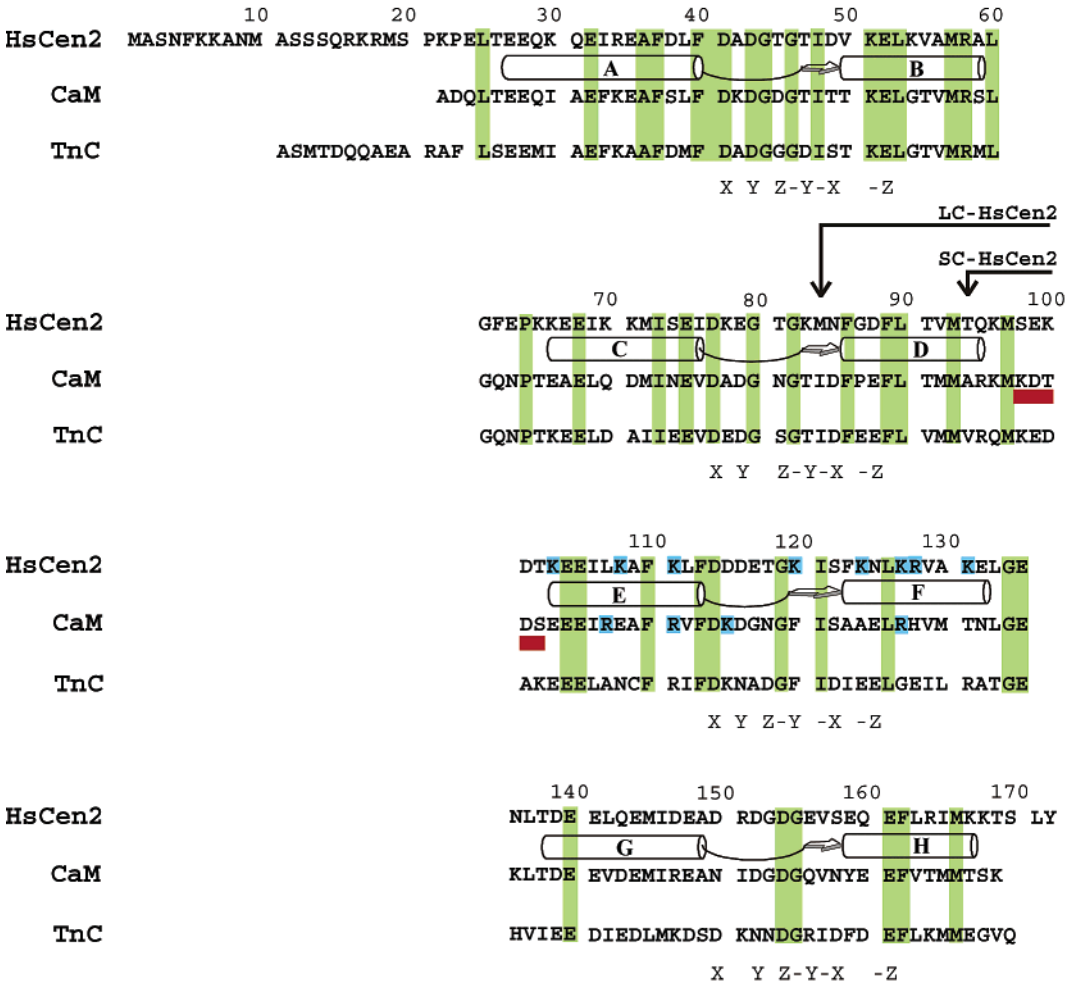

FIGURE 1: Sequence comparison of HsCen2 with *Drosophila melanogaster* CaM and chicken skeletal muscle TnC. Arrows show the start point of the two C-terminal fragments used in this work. Identical residues in HsCen2, CaM, and TnC are shown on a green background, and basic residues in EF-hand III in HsCen2 and CaM are shown on a blue background. The ligands of the metal ion are labeled in a standard manner corresponding approximately to a Cartesian coordinate system centered on Ca^{2+}. The elements of secondary structure and the calcium binding loops in CaM are also indicated. The red box underlines the interdomain fragment that is partially unwound in the solution structure of CaM.

human centrins requires a more detailed investigation of the conformational properties, Ca^{2+} binding, nature of the molecular target(s), and interaction mechanism.

We have undertaken studies of the structure/function relationships at a molecular level in one member of the subfamily: HsCen2. To avoid experimental difficulties related to the aggregation tendency of the integral protein, we concentrated our study on the isolated protein domains, primarily on the potentially regulatory domain including the last two EF-hand motifs (III and IV). To this aim, we expressed and purified the full-length protein and two C-terminal fragments: SC-HsCen2 (from Short C-terminal HsCen2) of 79 residues (T94-Y172, covering the two EF-hand sequence) and LC-HsCen2 (from Long C-terminal HsCen2) possessing 10 additional residues (the D-helix) on the N-terminal side (Figure 1). Ca^{2+} binding, Ca^{2+}-induced changes, and structural properties of these fragments were studied using flow dialysis and spectroscopic techniques in solution (CD, NMR, and fluorescence). The two polypeptides exhibit a large degree of conformational heterogeneity that is controlled by Ca^{2+} binding and the nature of the ionic composition of the solvent. Under certain conditions (Ca^{2+} loaded, 100 mM NaCl), LC-HsCen2 is sufficiently well-structured and stable to allow the elucidation of its three-dimensional structure. The domain exhibits a compact five-helix fold, in which the amphipatic D-helix interacts strongly with the hydrophobic groove, created by the two EF-hand motifs. The structural aspects of this intramolecular interaction, as well as the resulting increase in structural stability and Ca^{2+} affinity, show many similarities with the intermolecular interactions between Ca^{2+} sensor proteins and their targets.

MATERIALS AND METHODS

Protein Expression and Purification. The cDNA corresponding to HsCen2 and SC-HsCen2 genes were synthesized by Genaxis. Open reading frames were inserted into the vector pET24a(+) using both *Nde*I and *Eco*I restriction sites. Recombinant proteins were overexpressed using a vector under the control of T7 RNA polymerase and BL21(DE3) *Escherichia coli* strains. Cells were grown at 37 °C in a standard medium (Miller's LB Base) containing appropriated antibiotics and induced with IPTG (1 mM) for 3 h. For ^{15}N-labeled samples, we used a culture medium (M9) containing $(^{15}NH_4)_2SO_4$ (1.5 g/L) as the sole source of nitrogen, and the induction step with IPTG (0.1 mM) was prolonged to 18 h. Protein purification was done according to the procedure previously described (*15*). The shorter sequence

(T94-Y172), named SC-HsCen2, was directly overexpressed in *E. coli*, while the longer fragment (M84-Y172)[2], named LC-HsCen2, was obtained as a proteolysis product during the overexpression of the integral protein. Primary structure of the purified polypeptides was confirmed by N-terminal sequencing and mass spectrometry.

Ca^{2+} Binding. To remove contaminating bound cations, the protein samples were precipitated with 3% trichloroacetic acid and then passed through a 40 × 1 cm column equilibrated in 50 mM Tris-HCl, pH 7.5, and 150 mM KCl (buffer A). The final contamination was less than 0.05 Ca^{2+}/protein as determined by atomic absorption spectroscopy. Calcium binding was measured by flow dialysis at 25 °C in buffer A with protein concentrations of 20−30 μM, as described previously (*15*). Data treatment and evaluation of the intrinsic metal binding constants were done using the Adair equation for two or four binding sites (*16*). The intrinsic association constants, used for the presentation of the data, are linked to the macroscopic constants by the statistical factors 2 and $^1/_2$.

Chemical Denaturation. Urea denaturation was monitored by CD spectroscopy by recording far-UV spectra (200−250 nm) as a function of denaturant concentration. Proteins samples were 12 μM in 10 mM Tris-HCl buffer (pH = 7.6), 2 mM $CaCl_2$, 100 mM NaCl, at 25 °C, and increasing concentration of urea. The curves (ellipticity at 222 nm vs urea concentration) were normalized to give the fraction of unfolded molecules as a function of the denaturant concentration. The Gibbs free energy of the protein stability at a given urea concentration is given by the following relationship: $\Delta G^\circ = -RT \ln K$, where $K = F_u/(1 - F_u)$, and F_u is the unfolded fraction. It is reasonably supposed (*17*) that the Gibbs free energy is linearly dependent on the urea concentration $\Delta G^\circ = \Delta G^\circ_{H_2O} - m[\text{urea}]$, where m is a constant reflecting the strength of the dependence of the protein stability on denaturant concentration, and $\Delta G^\circ_{H_2O}$ is the extrapolated value of ΔG° at zero denaturant concentration. The normalized experimental curve may thus be fitted by the following expression:

$$F_u(x) = \frac{\exp[(mx - \Delta G^\circ_{H_2O})/RT]}{1 + \exp[(mx - \Delta G^\circ_{H_2O})/RT]}$$

to obtain m and $\Delta G^\circ_{H_2O}$.

NMR Spectroscopy. NMR samples (0.7−1.5 mM) were obtained by dissolving the lyophilized protein in deuterated Tris-HCl buffer (20 mM, pH 6.5) containing 100 mM KCl (or NaCl). NMR spectra were recorded on a Varian Unity 500 NMR spectrometer equipped with a triple probe and a Z-field gradient, at 308 K. Heteronuclear (^{15}N-^{1}H)-HSQC and (^{15}N-^{1}H)-NOESY-HSQC spectra were used to monitor Ca^{2+} titration and global characterization of SC-HsCen2 intermediates. Standard homonuclear experiments (COSY-DQF, TOCSY, and NOESY) in ^1H_2O or ^2H_2O were used for resonance assignment and collection of distance and angle restraints (*18*). Spectra analysis was carried out using Felix 230 software (Accelerys, San Diego, CA).

Structure Determination. Interproton distance restraints were obtained from NOESY spectra in ^1H_2O or ^2H_2O with mixing times of 100 and 150 ms. Two different samples, purified from different overexpression experiments, were comparatively analyzed to increase the confidence in identification of weak or ambiguous signals. Peak intensities were calibrated relative to NOEs corresponding to known interproton distances such as $H^N - H^N$ (2.8 Å in an α-helix) and $H^{\beta1} - H^{\beta2}$ (1.8 Å in methylene groups). The NOE restraints were classified into three categories: strong (1.8−3.0 Å), medium (3.0−3.8 Å), and weak (3.8−5.0 Å). Within the segments having a regular secondary structure, the observable distance restraints (like $d_{\alpha N}(i, i + 2)$ and $d_{NN}(i, i + 2)$, etc.) were confined to a range (±0.2 Å) around the standard distance characteristic to well-resolved structures (*18*). The final experimental restraints originate from the analysis of 1103 NOEs (∼13 per residue), 35 hydrogen bonds, and 103 dihedral angle data (see Table 1). No explicit restraint was used for the bound Ca^{2+} ions. With the exception of the fragment 164−166 (see the Results and Discussion section), we observed only a single NOE set, suggesting that the dimers are symmetric. In the absence of any detectable intermolecular NOE interactions, only a single molecule was considered in the structural modeling. The structures were generated with the Distance Geometry program (DGII, Accelrys, San Diego, CA). In the final run, after the optimization of the restraint file, we generated 200 course structures, using embedding and optimization steps. Seventy-six of these structures, which best satisfy the experimental restraints, were further refined by energy minimization (5000 steepest descent and 10 000 conjugated gradient steps) under the cvff force field of Discover. The final 25 structures were retained on the basis of the agreement with the experimental data and the low potential energy. The first structure in this assembly, which is closest to the average coordinates of the ensemble, was chosen as a representative conformer and used for structural illustration.

Fluorescence Spectroscopy. Changes of the fluorescence properties of TNS were monitored by fluorimetry as described previously (*19*). After incubation of 5 μM apo protein in buffer A containing either 20 μM EGTA or 2 mM Ca^{2+} with 40 μM TNS for 5 min, the solutions were excited at 328 nm, and the emission fluorescence spectra were recorded at 25 °C with 5 nm slits. The Ca^{2+} titrations were carried out on 5 μM metal-free protein in buffer A.

The interaction of SC-HsCen2 with ME was monitored by Trp fluorescence in an equimolar mixture of 10 μM protein and ME in Tris-HCl buffer (50 mM), pH 7.5, and KCl (150 mM). Excitation was done at 278 nm, and the two slits were fixed at 10 nm.

RESULTS AND DISCUSSION

The SC-HsCen2 fragment was designed so as to represent the C-terminal domain of HsCen2. In the Ca^{2+}-saturated crystal structures of CaM the linker between the two domains is α-helical, while in solution, experimental dynamics studies (*20*) revealed an unwound and highly flexible segment (77−81). In the structure of the isolated N-terminal domain (1ak8),

[2] Accession number: Coordinates corresponding to the 25 structures of the Ca^{2+}-saturated LC-HsCen2 (M84-Y172) have been deposited in the Protein Data Bank with the accession code 1M39. The first structure in this assembly, which is closest to the averaged coordinates of the ensemble, was chosen as a representative conformer. A file containing the proton assignment of the LC-HsCen2 domain was deposited in the BioMagResBank with the entry no. 5503.

Table 1: Restraint and Structural Statistics for the 25 Best Solution Structures of LC-HsCen2

Restraint statistics		
NOE restraints	1103	
intraresidue	354	32%
sequential	254	23%
medium range ($2 \leq \|i-j\| < 5$)	247	22%
long range ($\|i-j\| \geq 5$)	248	23%
hydrogen bond restraints	70	
dihedral angle restraints (Φ,Ψ)	103	
rms of NOE upper restraint violations	0.033 Å	
rms of NOE lower restraint violations	0.024 Å	
average number of distance restraint violations per structure (>0.2 Å)	4.1	
dihedral angle restraint violations	0	
	av. rmsd (Å) from the av. structure	
residues 105−113, 120−132, 139−148, 156−164[a]	0.47 (0.08)	
residues 86−94, 105−113, 120−132, 139−148, 156−164[a]	0.87 (0.3)	
EF-hand III[a]	0.59 (0.2)	
EF-hand IV [a]	0.64 (0.2)	
helix D[a]	0.26 (0.09)	
helix E[a]	0.17 (0.06)	
helix F[a]	0.18 (0.05)	
helix G[a]	0.14 (0.05)	
helix H[a]	0.19 (0.12)	
ensemble Ramachandran plot		
residues in the most-favored region	76.7%	
residues in additional allowed regions	16.4%	
residues in generously allowed regions	4.1%	
residues in disallowed regions	2.7%	

[a] Backbone atoms (N, C′, and C^{α}).

or in the target or drug complexes of CaM, determined both by NMR and X-ray (2bbn, 1cdl, 1cdm, 1ctr), the D helix is defined with a C-terminal end between M72 and R74, suggesting that the segment 72−81 has a weak propensity to organize in a regular structure and is flexible enough to allow the two domains to rearrange around various target peptides. The start of the SC-HsCen2 construct was chosen in the interdomain region of centrin 2 (T94), considering that a longer N-terminal sequence would be favorable for the stabilization of the E helix. The longer polypeptide (LC-HsCen2) was obtained as a spontaneous proteolysis product during the overproduction and purification in *E. coli* of the integral protein.

As the integral HsCen2 (*15*) or the *Chlamydomonas* centrin (*13*), the two C-terminal fragments have the tendency to self-associate. The NMR spectra of apo and Ca^{2+}-bound forms show global or local line broadening, more than in other proteins of similar size, which are more consistent with dimers or larger oligomers, in agreement with the analysis

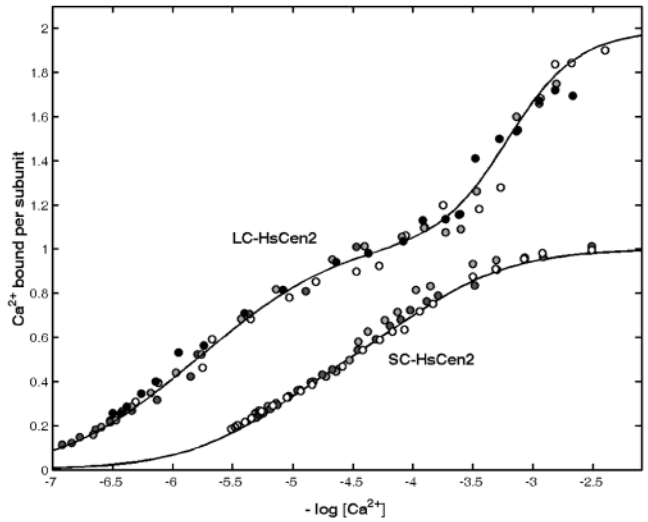

FIGURE 2: Ca^{2+} binding to LC-HsCen2 and SC-HsCen2 measured by flow dialysis. Experiments were performed at 25 °C in 50 mM Tris-HCl buffer, pH 7.5, and 150 mM KCl, using 25 μM protein concentration. The results of three independent assays are shown by marks of different styles.

of the flow dialysis or cross-linking experiments described below.

Ca^{2+} Binding. The Ca^{2+}-binding isotherm obtained by flow dialysis on 50 μM SC-HsCen2 (in Tris-HCl buffer and 150 mM KCl) indicated the binding of one Ca^{2+} per subunit with $[Ca^{2+}]_{0.5}$ of 29 μM and negative cooperativity, with a cooperativity constant n_H of 0.66 (Figure 2). When fitted to the Adair equation for two sites, the macroscopic binding constants are 1.5×10^5 and 8.1×10^3 M^{-1}, respectively. These binding parameters are very similar to those of full-length HsCen2 (*15*), indicating that the N-domain does not affect significantly the ion binding properties of the C-domain. The negative cooperativity further confirms that SC-HsCen2 is not monomeric, an observation confirmed by size-exclusion chromatography (data not shown).

The Ca^{2+}-binding isotherm of LC-HsCen2 revealed a completely different pattern of interaction with Ca^{2+} (Figure 2). Flow dialysis in buffer A containing 150 mM KCl revealed the binding of four Ca^{2+} ions per dimer at two different sets of sites: a pair with a $[Ca^{2+}]_{0.5}$ of 1.6 μM (18 times lower than for SC-HsCen2) and n_H of 1.0, and a second pair with a $[Ca^{2+}]_{0.5}$ of 640 μM, and n_H 2.0, indicating pronounced positive cooperativity ($n_H > 1$). Moreover, the nature of the monovalent cation in the buffer has a considerable influence on the Ca^{2+} binding of LC-HsCen2: the isotherm determined in the presence of 150 mM NaCl is also biphasic but is characterized by much lower $[Ca^{2+}]_{0.5}$ values of 0.26 and 209 μM, respectively. Therefore, the replacement of K^+ by Na^+ in the buffer leads to a 6- and 3-fold increase of the Ca^{2+} binding to high-affinity and low-affinity sites, respectively. The binding sites in SC-HsCen2 are also sensitive to the replacement of KCl by NaCl: they showed a 4-fold increase in affinity for Ca^{2+}.

Comparison with the closely related *Chlamydomonas* centrin (*13*) (71% sequence identity) shows that the C-terminal domains of the two proteins have similar calcium binding properties, with two sites of significantly different affinities (in the μM and mM ranges). In contrast, the N-terminal domains exhibit a distinct behavior: the binding

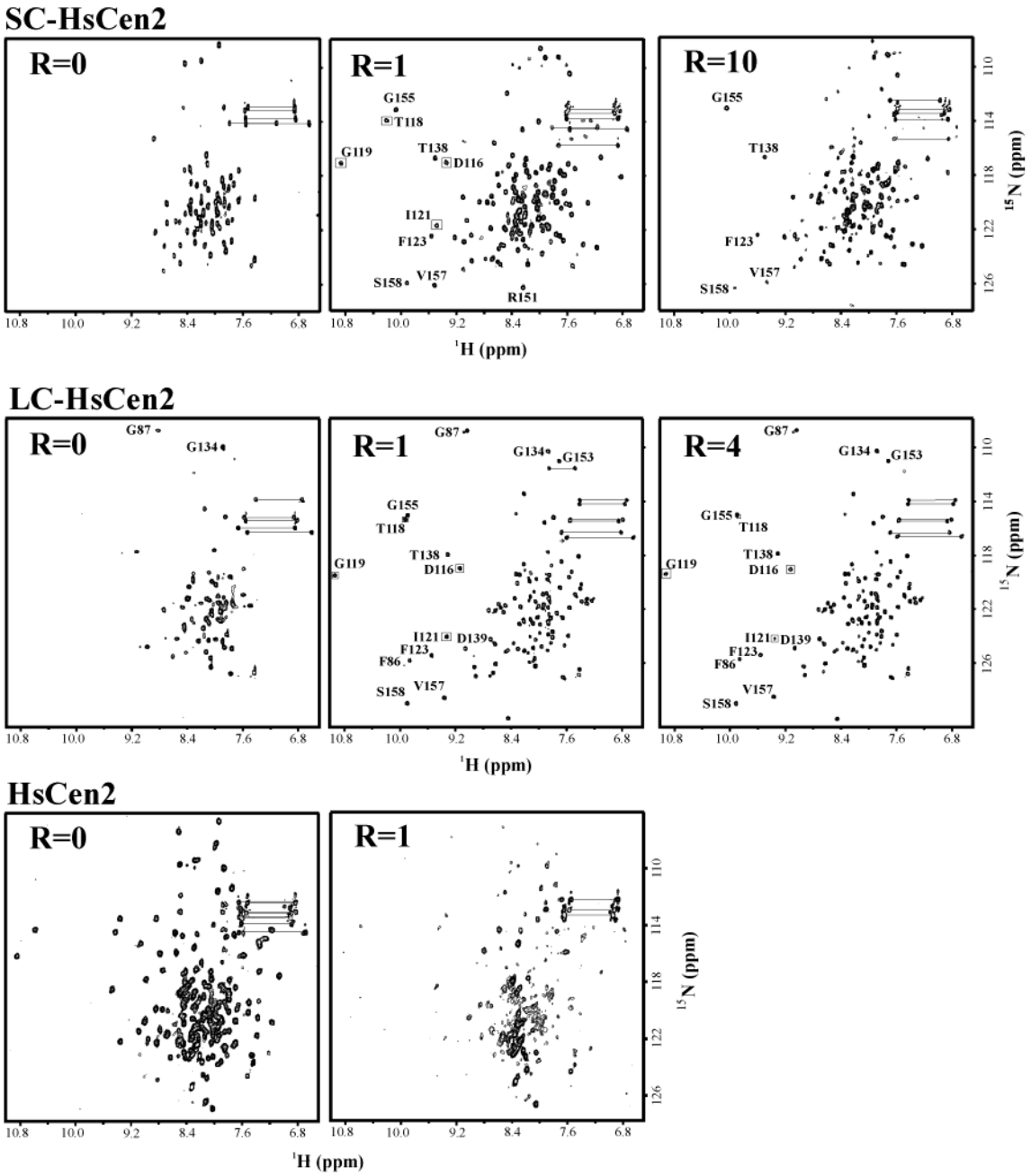

FIGURE 3: Ca^{2+} titration of SC-HsCen2, LC-HsCen2, and the integral protein (HsCen2) followed by NMR. ^{15}N-^{1}H-HSQC spectra of SC-HsCen2 (1.5 mM), LC-HsCen2 (1.3 mM), and HsCen2 (1.1 mM) in Tris-HCl (20 mM), pH 6.5, and NaCl (100 mM) were recorded in absence of Ca^{2+} (5 mM EDTA) or at various Ca^{2+}/protein molar ratios (R). Horizontal lines connect the pairs of cross-peaks corresponding to NH_2 groups in Asn and Gln side chains. Assignment of some low-field shifted peaks is shown. Boxed peaks, corresponding to the Ca^{2+}-binding loop III, undergo a large broadening during the second phase of titration. Spectra of SC-HsCen2 and HsCen2 were recorded at 25 °C, while the spectra of LC-HsCen2 were recorded at 35 °C.

affinity of the *Chlamidomonas* domain is similar to that observed for Ca^{2+} sensors, while the HsCen2 appears to be insensitive to divalent cations. The fact that a number of amino acids in the first binding loops of HsCen2 (one in loop I and four in loop II) are rarely encountered in the known EF-hand sequences (*25*) could be related to the low affinity of the N-terminal domain. The role of the N-terminal sequence, which is longer in centrin sequences, should also be investigated for its possible influence on structural and functional properties of this EF-hand subfamily.

Ca^{2+}-Induced Conformational Changes. In the absence of calcium, both C-terminal domains of human centrin 2 (SC-HsCen2 and LC-HsCen2) exhibit a high conformational disorder, characterized by the presence of elements of secondary structure (observed by far-UV CD spectra) but the absence of persistent tertiary interactions, as reflected in a poor spectral dispersion and lack of long-range NOEs in NMR spectra. The (^{15}N-^{1}H)-HSQC spectra of SC-HsCen2 and LC-HsCen2 (Figure 3) contain a number of distinct NH peaks compatible with the polypeptide sequences, distributed within a narrow spectral range in the amide proton dimension (between 7.3 and 9.0 ppm), suggesting weak (or absence) intramolecular hydrogen bonds, a lack of persistent secondary structure and fluctuating ring current effects. These spectral features are independent of the nature of the cation in the buffer (KCl or NaCl, 100 mM). Similar observations were

made on other apo EF-hand domains such as the C-terminal halves of muscle troponin C (TnC) (*21*), CaVP (*22*), and the NSCP (*23*), which were considered to be in a molten globule state. However, the observation of sharp NMR resonances is not consistent with a molten globule state for these constructs.

The HSQC spectrum of the integral protein in the absence of Ca^{2+} has a more complex pattern, with well-dispersed and moderately broadened peaks (about half of the expected peaks), coexisting with a crowded central region. By comparison with the apo C-terminal fragments, it may be inferred that the N-terminal half of the integral protein is largely folded, but this is not enough to stabilize the other half. A similar case was recently described in our laboratory for another EF-hand protein, Calcium Vector Protein (*24*).

To estimate the pattern and the amplitude of Ca^{2+}-induced conformational changes, we titrated ^{15}N uniformly labeled SC-HsCen2 and LC-HsCen2 (in Tris-HCl (20 mM), pH 6.5, and KCl (100 mM)) by Ca^{2+} and analyzed the corresponding (^{15}N-^{1}H)-HSQC spectra. Addition of substoichiometric concentrations of Ca^{2+} to the protein solution induces a dramatic increase in the frequency range of amide proton resonances (mainly in the proton dimension), indicating the stabilization of the tertiary fold. However, even at a high cation/protein ratio (4 or 6), the majority of the observed cross-peaks are broadened, probably because of a slow-to-intermediate exchange between bound and free conformations. When KCl is replaced by NaCl in the buffer, the quality of the spectra improved significantly, and the Ca^{2+} titration evolves differently. From the beginning of the titration, the spectral range in the proton dimension increases by a factor of 2 (Figure 3), indicating the presence of regular three-dimensional conformations involving backbone hydrogen bonds and large ring current effects. Up to 1 equiv of Ca^{2+}, the number of observed cross-peaks in the HSQC spectra, is larger than that expected from the sequence, suggesting a slow exchange (on the order of 10 s^{-1} or less) between free and bound conformations. Increased affinity, via a slower off rate constant, may explain the change in dynamic behavior in the presence of sodium ions. The need of high Na^{+} concentration (on the order of 100 mM) suggests that the stabilizing effect is mediated by diffuse Na^{+} interactions with negative charges at the protein surface rather than by binding at specific sites.

Some of the low-field-shifted resonances could be assigned, based on a 3-D NOESY-HSQC spectrum, and by comparison with the almost complete assignment of LC-HsCen2 (see below) and of bimolecular complexes of SC-HsCen2 [Miron, S., and Craescu, C. T., unpublished results]. Thus, the peaks at 10.85 and 10.07 ppm were assigned to the HN group of G119 and G155, respectively (Figure 3). The large shift of these amide protons, belonging to the sixth residue in the canonical Ca^{2+}-binding loop, is due to a strong hydrogen bond with a carboxyl oxygen of the first residue in the loop, usually an Asp residue. Such intraloop interactions were observed in all the Ca^{2+}-bound EF-hands (*25*) but also in at least one apo structure (*24*). The present spectral observations indicate that formation of the intraloop hydrogen bonds C′O(1)−HN(6) in both EF-hands takes place from the very beginning of the titration.

Because of the direct Ca^{2+} binding to the neighboring backbone carbonyl oxygen, the amide nitrogen resonance of the eighth residue in the binding loop is a sensitive probe for the individual coordination state of EF-hand domains (*26*). According to the ^{15}N chemical shifts of the corresponding residues in SC-HsCen2 and LC-HsCen2 (122.0 ppm for I121 and 126.2 ppm for V157), it may be inferred that EF-hand III and IV are in the apo and bound states, respectively, in the presence of 1 Ca^{2+} equiv. The large difference in affinity between the two EF-hand motifs, observed in the NMR titration, is in good agreement with the flow dialysis results and with the better conservation of the consensus binding sequence in site IV. Therefore, binding of the first Ca^{2+} ion by site IV induces a significant stabilization of the structure of both EF-hand motifs.

During the second part of the titration of SC-HsCen2, between 1 and 13 Ca^{2+} equiv, a number of cross-peaks, corresponding to the loop III residues (D116, T118, G119, and I121, boxed in Figure 3), exhibit a progressive broadening and finally disappear. Binding of the second Ca^{2+} ion is thus associated with a faster exchange process, on an intermediate time scale relative to the frequency difference between conformers. During the final stage of the titration, exchange broadening at similar or faster rates were also observed for EF-hand IV resonances, as may be observed for S158 and V157 (Figure 3). The final HSQC spectrum exhibits peaks of variable intensity, suggesting a conformational disorder-induced line broadening, extending over the whole domain. The NOESY experiment gives low quality spectra that can be hardly used for a structural analysis. These observations show that, even in excess of Ca^{2+}, the domain remains conformationally heterogeneous and can dynamically explore two or more conformational states, depending on the binding state as well as on the nature and concentration of the buffer salt. This level of conformational disorder is inappropriate for the X-ray or NMR procedures of structure determination.

In contrast with the shorter domain, LC-HsCen2 in the presence of Ca^{2+} excess and 100 mM Na^{+} shows HSQC spectra of better quality (Figure 3) containing the number of cross-peaks expected from the primary structure. The spectral dispersion and observation of a coherent ensemble of short- and long-range NOE connectivities indicate that this fragment exhibits a unique and persistent three-dimensional structure that can be determined using NMR spectroscopy. However, several resonances including D116, T118, G119, and I121 (boxed in Figure 3) show a Ca^{2+}-sensitive broadening (smaller than in SC-HsCen2) during the second half of the titration, suggesting that the binding loop III still shows a slight conformational heterogeneity.

Ca^{2+} titration of the integral HsCen2 revealed a different behavior: binding of the divalent cations induces a progressive spectral degradation, mainly because of a general line broadening. The calcium-induced spectral changes observed for HsCen2 are most probably because of the protein aggregation and were also noted in the case of *C. reinhardtii* centrin (*13*).

The Ca^{2+}-induced structural changes in the C-terminal fragments were further investigated using the hydrophobic fluorescent probe, TNS. In presence of apo SC-HsCen2 (Figure 4) and LC-HsCen2 (not shown), the fluorescence of the probe, at μM concentration, is enhanced by a factor of 3.5 and 3, respectively. The observed changes are similar to those induced by HsCen2, but at 2−3-fold higher protein

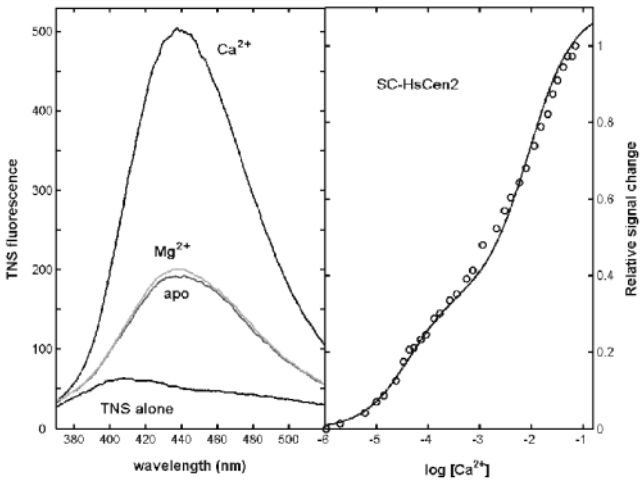

FIGURE 4: TNS fluorescence enhancement. The figure illustrates the case of SC-HsCen2 at 25 °C in 50 mM Tris-HCl, pH 7.5, and 150 mM KCl. Left panel: Fluorescence spectra of TNS alone or in the presence of SC-HsCen2 and 2 mM Ca^{2+}, SC-HsCen2 and 20 μM EGTA, or SC-HsCen2 and 2 mM Mg^{2+}. Right panel: Titration of the mixture of 5 μM metal-free protein and 40 μM TNS by Ca^{2+}. The normalized signal changes show a first transition at $[Ca^{2+}]_{0.5} = 30$ μM and a second transition at $[Ca^{2+}]_{0.5} = 8$ mM.

concentrations, suggesting that in full-length centrin the N-domain has a significant contribution to the probe fluorescence enhancement reported previously (*15*).

The Ca^{2+}-induced changes observed in NMR spectra of SC-HsCen2 are accompanied by a larger (8-fold) TNS fluorescence enhancement, most likely because of an increase of the exposed hydrophobic surface (Figure 4). A Ca^{2+} titration of SC-HsCen2 revealed two main steps in the fluorescence enhancement of the probe: 35% of the total increase occurs with $[Ca^{2+}]_{0.5}$ of 30 μM and 65% with a $[Ca^{2+}]_{0.5}$ of 8 mM (Figure 4, right panel), similar to the case of the integral protein (*15*). The significant increase of the exposed hydrophobic patch upon metal binding is a general trend of the regulatory Ca^{2+}-binding domains (*27*).

In contrast with SC-HsCen2, the Ca^{2+}-loaded LC-HsCen2 shows only a 1.5-fold additional fluorescence enhancement, and only at high (mM) Ca^{2+} concentrations, indicating that the hydrophobic TNS binding surface is considerably lower.

Structure of LC-HsCen2. The proton resonance assignment of LC-HsCen2 in the Ca^{2+}-saturated state (20 mM $CaCl_2$) was done using the standard homonuclear sequential assignment procedure. Resonances from residues between K96 and T102 remained unassigned, probably because of an intermediate-to-slow conformational exchange, resulting in very broad peaks. Cross-peaks involving residues R164-M166 are also affected, either broader or appearing as a pair, indicating slow exchange between alternative conformations. Finally, protons from the C-terminal segment (K167-Y172) give only short-range NOE connectivities, likely becasue of an increased flexibility, and their assignment is ambiguous. Overall, resonances for 79 of the 89 residues have been assigned, including backbone and side-chain protons.

Combined analysis of short- and medium-range NOEs between backbone protons and of secondary chemical shift of H^{α} protons enabled us to delineate five α-helices, F86-T94, E105-F113, F123-E132, D139-A148, and E159-R164 (representing helices D, E, F, G, and H, respectively), and a two-stranded (K120-S122 and E156-S158) antiparallel β-sheet. Helices D, E, and H are shorter than expected from a prediction based on sequence alignment with related proteins of known structure (Figure 1). According to the relative exchange kinetics ($^1H/^2H$) of the amide protons (estimated from several TOCSY spectra, recorded after sample lyophilization and dissolving in ^2H_2O), the G helix seems to be the most stable helix in this domain. Resonances of the amide protons in G119 and G155 (position 6 in Ca^{2+} loops) are highly downfield shifted at 10.95 and 9.90 ppm, respectively. Combined with a slower $^1H/^2H$ exchange rate, this is a strong indication for the existence of the canonical intraloop C′O-(1)−HN(6) hydrogen bond in both EF-hand motifs.

Figure 5a shows the superimposition of the 25 final structures calculated from the 1276 NMR restraints. There is no distance restraint violation larger than 0.4 Å and no violation of dihedral angle restraints. A total of 97.2% of all residues have on average their backbone dihedral angles in the allowed regions of the Ramachandran plot (Table 1). Procheck-NMR (*28*) analysis indicates that the global quality of the determined structure is comparable to a crystallographic structure at 2.5 Å resolution. The restraint and structural statistics are summarized in Table 1.

The coupled EF-hand motifs form a canonical structure, similar to other Ca^{2+}-bound domains from the family. The backbone is well-defined with root-mean-square (rms) deviations from the mean of 0.47 (±0.08) Å for the helices E−H and the β-strands but increases to 0.87 (±0.3) when helix D is included. The α-helices within each EF-hand motif are almost perpendicular, a characteristic of the Ca^{2+}-bound (open) states of regulatory Ca^{2+} binding proteins (*29*). The mean interhelical angles (*27*) in the present conformational ensemble are 104 (±5)° and 84 (±5)° for the EF-hand III and IV, respectively, similar to the corresponding values in the C-terminal domain of CaM$(Ca^{2+})_2$ (101 and 94°) (*30*). In this open fold, many apolar residues (I106, A109, F110, F113, I121, L126, V129, L133, L137, M145, V157, F162, and I165) cover the deep central cavity giving it a pronounced hydrophobic character (Figure 5c). These residues are identical in CaM (with the exception of I165, which corresponds to a Met in CaM), suggesting a high evolutionary pressure for the conservation of the apolar character of this surface. Despite this common property, mainly required for the hydrophobic interaction with the target, the regulatory proteins from the CaM super family may accomplish distinct functions according to their localization, specific Ca^{2+}-binding parameters (affinity, kinetic constant, and cooperativity), target recognition, and target-bound conformation.

The N-terminal segment, including the D helix (F86-T94), is not freely moving in the solvent outside the main structure but lies down over the hydrophobic groove with its apolar side chains protruding deeply inside the structure. The wheel projection (Figure 5d) reveals the well-defined amphipatic character of the helix with hydrophobic side chains (F86, F89, L90, V92, and M93) on the inner face and polar or acidic side chains on the outer face. Most of the interactions between the D-helix and the protein core (38 of the 42 long-distance NOEs) involve F86, F89, and M93 (Figure 5c). They interact mainly with hydrophobic side chains from EF-hand III (F113, I121, L126, A130, and L133), and to a lesser extent, from EF-hand IV (L142 and V157). In fact, the complexes formed by the C-terminal domain of homologous proteins share a common binding site, constituted by helix

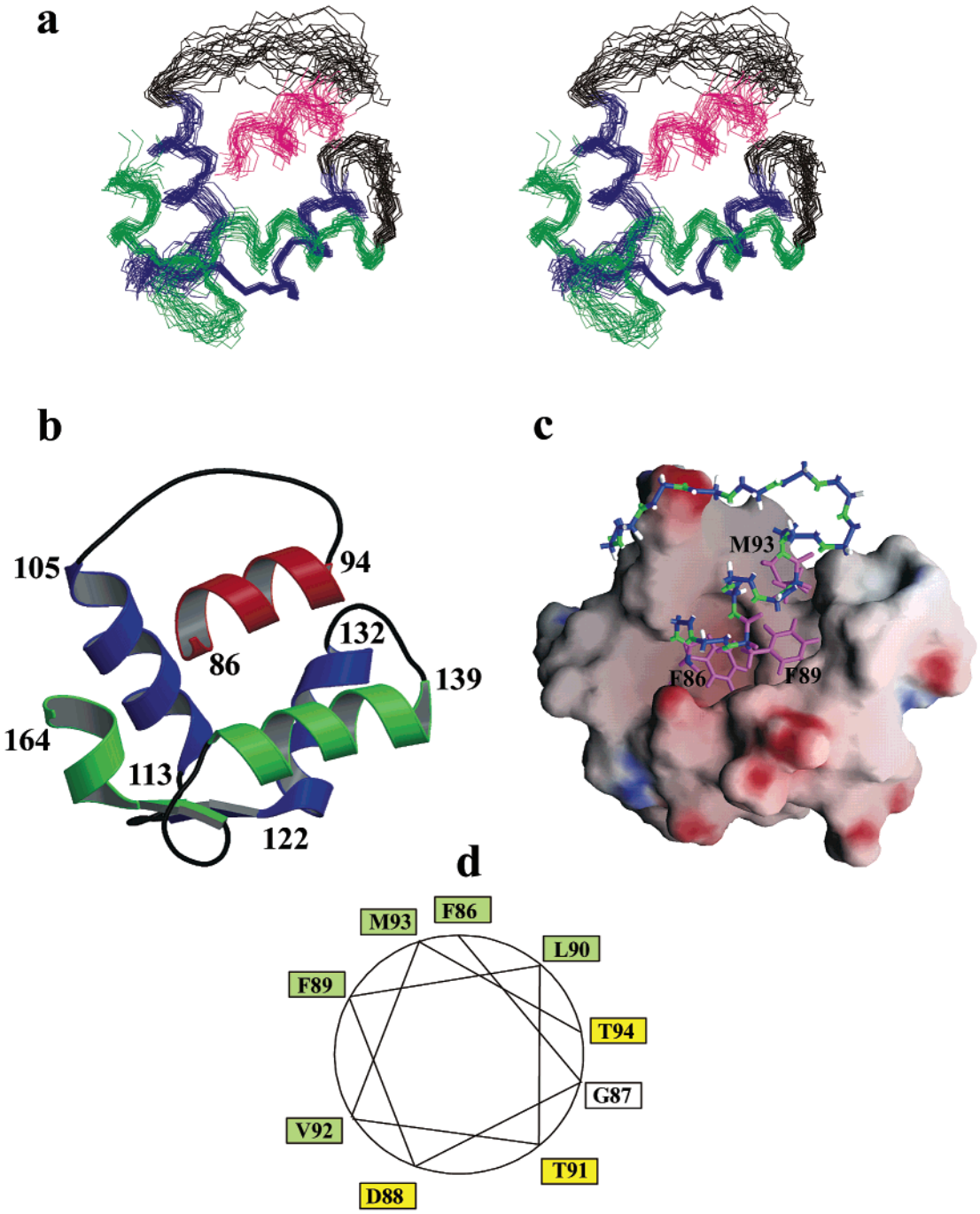

FIGURE 5: Solution structure of LC-HsCen2. (a) Stereo representation of the superimposition (using the segments 86−94, 105−113, 120−132, 139−148, 156−164, and backbone heavy atoms N, C′, and C^{α}) of the 25 final structures of LC-HsCen2 in the Ca^{2+}-saturated state. (b) Ribon representation of the solution structure of Ca^{2+}-bound LC-HsCen2 domain using the coordinates of the structure that is closest to the average coordinates of the ensemble, prepared with MOLSCRIPT and Raster 3D software. Helices from the third and fourth EF-hand motifs are colored in blue and green, respectively, the helix D is colored in magenta, and the linker fragments are black. (c) Electrostatic potential calculated at the molecular surface for the fragment 105−165 using GRASP software (*44*) and the stick representation of the backbone of segment 86−104. Positive and negative potentials are shown in blue and red, respectively. For simplification reasons, only F86, F89, and M93 side chains of hydrophobic residues in the D-helix are shown. (d) Wheel representation of the segment F86-T94, showing the amphipatic character of the α-helix.

E, the inter-motif linker and helix H (*31*). The different peptides are bound in two symmetric orientations relative to the C-terminal half of CaM, and in our construct the D-helix shows the same polarity as the myosin light chain kinase peptides (*32*, *33*) or the CaMKII peptide (*34*) but a reversed polarity relative to the CaMKK peptide (*35*).

The intramolecular interaction between the main domain and the D-helix could give useful indications on the capacity of HsCen2 to recognize and bind its molecular target(s). It has been early proposed that the prototype CaM-binding domain is a short amphiphilic α-helix with a basic hydrophilic face (*36*). Sequence analysis of a large number of CaM targets (*37*, *38*) and of available 3-D structures of CaM/target complexes resulted in identification of four main classes of consensus sequence patterns. Three of them, encountered in Ca^{2+}-dependent interactions, are distinguished

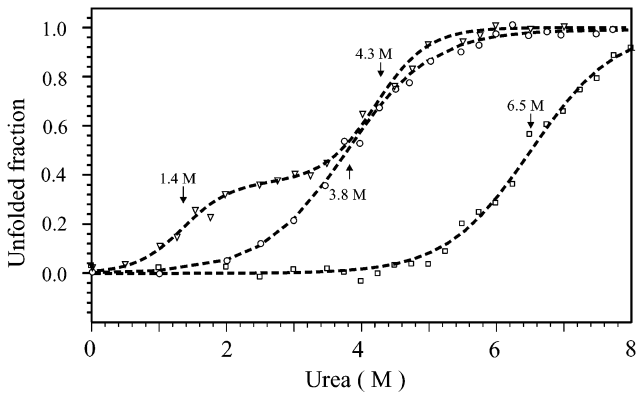

FIGURE 6: Urea unfolding curves. Intact HsCen2 (triangles) and two C-terminal fragments, SC-HsCen2 (circles) and LC-HsCen2 (squares), were studied in Tris-HCl buffer, pH 7.6, 2 mM $CaCl_2$, and 100 mM NaCl at 25 °C. Normalized unfolded fractions, estimated from far-UV ellipticity at 222 nm, are represented as a function of urea concentration. Arrows indicate the C_m values for different unfolding processes.

by a specific spacing of interacting bulk hydrophobic residues: 1−10, 1−14, and 1−16. The hydrophobic side chains from the D-helix define a 1−4−5−8 pattern (where the numbers indicate the position of bulky hydrophobic residues in the sequence starting with F86), which is similar to the subclass 1−5−10 (including CaMKI and CaMKII and NO synthase) of CaM binding sites (*38*). However, unlike these sequences, the D-helix includes a negatively charged side chain and no basic residues. It was hypothesized that the positively charged side chains in most CaM binding domains contribute to the binding energy by electrostatic interactions with negative charges on CaM (*39*). The present structure of LC-HsCen2 proves that the helix/EF-hand domain interaction may exist without a significant electrostatic component. The fact that the binding peptide is already in the proximity of the domain (even tethered to the polypeptide chain) and is not dissociable should also contribute to the increased affinity and stability of the complex in this particular case (*40*). In this respect, it should be noted that EF-hand III in HsCen2 is considerably less acidic than in CaM, essentially because of a larger number of basic residues (Figure 1). This charge property predicts that human centrin may preferentially recognize amphipatic helices with a lower basic character. This provides a contrast to the strong similarity of the hydrophobic surfaces and may suggest how CaM and HsCen2 are able to function in independently regulatory pathways.

Structural Stability. Using urea as a chemical agent and far-UV CD spectroscopy to estimate the secondary structure content, we analyzed the unfolding of HsCen2 and of the two C-terminal fragments (Figure 6) in the Ca^{2+}-saturated form. The best fit of the experimental data gives the intrinsic free energy of unfolding ($\Delta G^\circ_{H_2O}$), and *m*, a measure of the dependence of ΔG° on denaturant concentration. The unfolding profile of the intact protein shows a well-defined two-step process, with distinct midpoint concentrations (C_m are 1.4 and 4.3 M) and free energy of stability ($\Delta G^\circ_{H_2O}$ are 2.4 ± 0.6 and 6.5 ± 1 kcal/mol, respectively). It may be reasonably assumed that the two halves of HsCen2 have clearly different structural stabilities and unfold in a sequential manner. This assumption is further supported by the unfolding profile of the shorter C-terminal fragment that shows a single step transition with a C_m of 3.8 M (Figure 6), close to the value of the second unfolding step of the integral protein. Therefore, the N-terminal domain, which represents the first unfolding unit, has a lower stability, similar to that of the EF-hand domains in Ca^{2+}-free CaM (*41*). Despite similar values for C_m, the free energy of stability ($\Delta G^\circ_{H_2O}$) of the isolated C-terminal domain is about two times lower (3.5 ± 0.2 kcal/mol) than that measured in the integral protein. A similar difference in stability between the isolated C-terminal domain and its counterpart in the intact protein was also observed in holo-CaM (*41*), but the reverse was observed in the apo form (*41*, *42*). The explanation should take into account a number of complex factors including the relative Ca^{2+} affinities, the possible unfolding pathways, the additional intramolecular interactions in the integral protein, and the particular design of the isolated domains.

Urea unfolding of the LC-HsCen2 reveals a distinctly higher structural stability (C_m = 6.5 M, $\Delta G^\circ_{H_2O}$ = 6.0 ± 0.3 kcal/mol) relative to the shorter fragment and to the whole centrin. Obviously, this increased stability must be related to the energetically favorable interaction between the tethered D-helix segment and the EF-hand domain. The hydrophobic patch, exposed to the solvent in SC-HsCen2 (a destabilizing factor), is now complemented by the apolar face of the D-helix, forming a more stable structure. A similar increase in structural stability should be observed in the case of target binding in cellular conditions. Preliminary experiments performed in our laboratory (Craescu, C. T., unpublished results) showed that, in complex with an amphiphilic peptide, the Ca^{2+}-bound SC-HsCen2 exhibits a cooperative thermal unfolding process at about 83 °C, while the uncomplexed domain unfolds over a wide temperature range with a mid-temperature of about 65 °C.

Melittin Binding. Melittin (ME), a 26-residue peptide, extracted from the bee venom, is considered a good model for the binding sites of CaM targets (*43*). Using the emission fluorescence of the single Trp residue in ME, we have recently shown (*15*) that full-length HsCen2 forms, in a Ca^{2+}-dependent manner, a 1:1 high-affinity complex with this model peptide ($K_a = 1.0 \times 10^7$ M^{-1}, the binding energy $\Delta G = -9.7$ kcal/mol). It is interesting to note that this stoichiometry is different from that observed for *Chlamydomonas* centrin (*13*), which is capable of binding simultaneously two amphiphilic peptides derived from the yeast Kar1p protein. In the present study, we focused on the binding capacity of the two C-terminal domains. Addition of 1 equiv of SC-HsCen2 to a solution of ME in the presence of Ca^{2+} (1 mM) leads to a blue shift of the fluorescence emission from 350 to 329 nm and a 2-fold increase of the fluorescence intensity of the Trp residue (Figure 7). Titration of ME (at 10 μM) by SC-HsCen2 reveals the formation of a 1:1 complex with an affinity constant K_a of 0.5×10^7 M^{-1} and a corresponding free energy of $\Delta G = -9.3$ kcal/mol, which represents 96% from that of the integral protein. This suggests strongly that the C-terminal domain plays a central role in target binding to HsCen2. The apo SC-HsCen2 induces a smaller blue shift (15 nm) and no significant fluorescence increase, indicating the Ca^{2+} dependence of the interaction.

In contrast with SC-HsCen2, addition of up to 30 μM of Ca^{2+}-bound LC-HsCen2 to 10 μM ME induces only a 5 nm

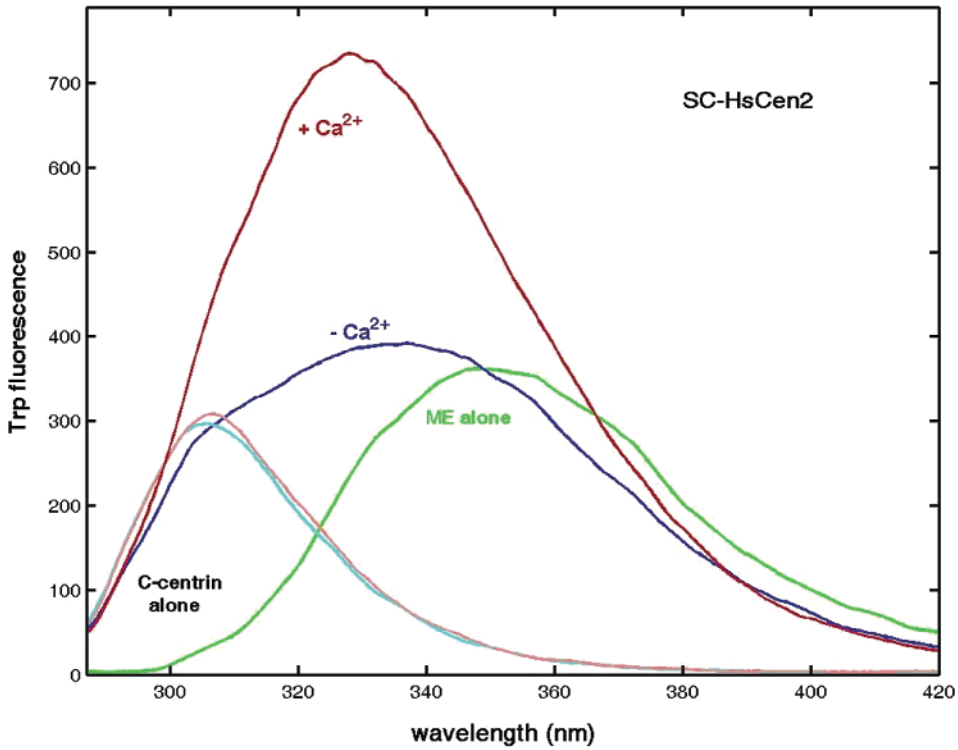

FIGURE 7: Interactions between SC-HsCen2 and melittin. Fluorescence emission spectrum of the Trp side chain in melittin (10 μM) is recorded in absence (green) and presence of Ca^{2+}-bound (red) and Ca^{2+}-free (blue) SC-HsCen2 (10 μM). The fluorescence emission spectra of SC-HsCen2 in the presence and absence of Ca^{2+} are shown at the left part of the figure. Samples are in Tris-HCl buffer (50 mM), pH 7.5, and KCl (150 mM).

blue shift (the same as was observed in the presence of 50 μM EGTA) but no significant fluorescence enhancement. The inability of LC-HsCen2 to bind ME is most probably because of the competition between the D-helix and the peptide for the same binding pocket, the D-helix having a higher affinity.

The Ca^{2+}-loaded HsCen2 has the tendency to form oligomers, but in the presence of ME the equilibrium is shifted toward monomers through the formation of a 1:1 HsCen2/ME complex (*15*). To characterize the binding pattern of SC-HsCen2, which appears to form dimers in the Ca^{2+}-bound state, we used chemical cross-linking experiments. The complex formed in the presence of Ca^{2+} was stabilized by covalent cross-linking with suberic acid bis-(*N*-hydroxysuccinimide ester) (DSS) and studied by SDS−PAGE. In the presence of DSS, SC-HsCen2 alone shows distinctly the dimer band as well as traces of oligomers. Upon increasing the ME/protein ratio from 0.5 to 2, the dimer and oligomer bands disappear in favor of a monomer band with an electrophoretic mobility corresponding to the molecular mass of the complex. Thus, the short C-terminal construct of HsCen2 characterized in the present study exhibits Ca^{2+} and peptide binding properties similar to those observed for the integral protein. These observations emphasize the important functional role played by the C-terminal domain in human centrin 2 and support the functional relevance of the SC-HsCen2 construct designed to represent it.

Biological Implications. Despite a similar structural organization, the proteins of the EF-hand superfamily accomplish distinct and diverse cellular functions, mainly because of differences in primary structure that control structural flexibility, target specificity, and binding energetics. Detailed structural and dynamic studies in various binding states should help establish comprehensive relationships between sequence, structure, dynamics, and function of these proteins. The data reported here show that HsCen2, and particularly its C-terminal domain, is only partly stabilized by Ca^{2+} and monovalent cations.

The two different constructs used in the present study proved to be complementary in modeling the C-terminal features of the C-terminal domain of HsCen2. Although not enough stabilized by Ca^{2+} binding, and thus not appropriate for the structure determination procedure, the shorter fragment (SC-HsCen2) showed peptide binding parameters that account for the binding capacity of the whole protein. On the other hand, utilization of the longer fragment allowed us to obtain structural information on the Ca^{2+}-bound state and to identify regulatory-type properties. NMR titration experiments revealed that, depending on the Ca^{2+} or K^+/Na^+ concentration in the medium, HsCen2 could explore several thermodynamic states, each representing an equilibrium (on intermediate NMR time scale) of more or less distinct conformations. The lack of a well-folded, stabilized structure of HsCen2 may be an advantage in recognizing various target molecules. At present, centrins are unique in this respect since domains in other EF-hand proteins, like CaM and calcineurin B, are distinctly more stable in the apo form and exhibit stabilized well-folded conformations. The structure of LC-HsCen2, determined here, represents one of the possible conformations explored by human centrins in the physiological medium and may be close to that assumed in the presence of a target molecule. Preliminary results of a study, aiming to characterize the complex of SC-HsCen with an amphiphilic peptide, derived from a possible protein target of human centrin, show that the short C-terminal domain in the complex exhibits similar secondary structure

and tertiary interactions as the corresponding fragment from LC-HsCen2 (Miron, S., and Craescu, C. T., unpublished results). From the structural properties discussed here, we anticipate that HsCen2/target complexes are of lower affinity than those with the more rigid CaM and TnC, etc., and this was indeed the case for the model peptide ME (*15*).

A number of structural and functional properties of the C-terminal fragments reported in this and previous studies enable us to assign a Ca^{2+} sensor function to HsCen2, with the regulatory role being mainly accomplished by the C-terminal domain. Among these properties, the Ca^{2+}-induced conformational changes, the open liganded structure, exposure of a large hydrophobic patch, and binding of amphiphilic peptides are the most relevant. All these features seem to be largely independent of the N-terminal half that may play different roles in stability, localization, or functional assembly within the centrosome environment.

ACKNOWLEDGMENT

We thank Cristina Niculescu for her contribution to the denaturation experiments.

REFERENCES

1. Lingle, W. L., Lutz, W. H., Ingle, J. N., Maihle, N. J., and Salisbury, J. L. (1998) Centrosome hypertrophy in human breast tumors: implications for genomic stability and cell polarity, *Proc. Natl. Acad. Sci. U.S.A. 95*, 2950−2955.
2. Lingle, W. L., Barrett, S. L., Negron, V. C., D'Assoro, A. B., Boeneman, K., Wanguo, L., Whitehead, C. M., Reynolds, C., and Salisbury, J. L. (2002) Centrosome amplification drives chromosomal instability in breast tumor development, *Proc. Natl. Acad. Sci. U.S.A. 99*, 1978−1983.
3. Urbani, L., and Stearns, T. (1999) The centrosome, *Curr. Biol. 9*, R315−R317.
4. Salisbury, J. L. (1995) Centrin, centrosomes, and mitotic spindle poles, *Curr. Opin. Cell Biol. 7*, 39−45.
5. Errabolu, R., Sanders, M. A., and Salisbury, J. L. (1994) Cloning of a cDNA encoding human centrin, an EF-hand protein of centrosomes and mitotic spindle poles, *J. Cell Sci. 107*, 9−16.
6. Lee, V. D., and Huang, B. (1993) Molecular cloning and centrosomal localization of human caltractin, *Proc. Natl. Acad. Sci. U.S.A.* 90, 11039−11043.
7. Middendorp, S., Paoletti, A., Schiebel, E., and Bornens, M. (1997) Identification of a new mammalian centrin gene, more closely related to *Saccharomyces cerevisiae* CDC31 gene, *Proc. Natl. Acad. Sci. U.S.A. 94*, 9141−9146.
8. Araki, M., Masutani, C., Takemura, M., Uchida, A., Sugasawa, K., Kondoh, J., Ohkuma, Y., and Hanaoka, F. (2001) Centrosome protein centrin 2/caltractin 1 is part of the *Xeroderma Pigmentosum* group C complex that initiates global genome nucleotide excision repair, *J. Biol. Chem. 276*, 18665−18672.
9. Middendorp, S., Küntzinger, T., Abraham, Y., Holmes, S., Bordes, N., Paintrand, M., Paoletti, A., and Bornens, M. (2000) A role for centrin 3 in centrosome reproduction, *J. Cell Biol. 148*, 405−415.
10. Wiech, H., Geier, B. M., Paschke, T., Spang, A., Grein, K., Steinkötter, J., Melkonian, M., and Schiebel, E. (1996) Characterization of green alga, yeast, and human centrins, *J. Biol. Chem. 271*, 22453−22461.
11. Schiebel, E., and Bornens, M. (1995) In search of a function for centrins, *Trends Cell Biol. 5*, 197−201.
12. Weber, C., Lee, V. D., Chazin, W. J., and Huang, B. (1994) High level expression in *Escherichia coli* and characterization of the EF-hand calcium-binding protein caltractin, *J. Biol. Chem. 269*, 15795−15802.
13. Veeraraghavan, S., Fagan, P. A., Hu, H., Lee, V., Harper, J. F., Huang B., and Chazin, W. J. (2002) Structural independence of the two EF-hand domains of caltractin, *J. Biol. Chem. 277*, 28564−28571.
14. Pastrana-Rios, B., Ocaña, W., Rios, M., Vargas, G. L., Ysa, G., Poynter, G., Tapia, J., and Salisbury, J. L. (2002) Centrin: its secondary structure in the presence and absence of cations, *Biochemistry 41*, 6911−6919.
15. Durussel, I., Blouquit, Y., Middendorp, S., Craescu, C. T., and Cox, J. A. (2000) Cation- and peptide-binding properties of human centrin 2, *FEBS Lett. 472*, 208−212.
16. Cox, J. A. (1996) Techniques to Measure the Binding of Ca^{2+} and Mg^{2+} to calcium-binding proteins, in *Guidebook to the Calcium-Binding Proteins* (Celio, M. R., Pauls, T., and Schwaller, B. Eds.) pp 1−12, Oxford University Press, Oxford.
17. Pace, C. N. (1986) Determination and analysis of urea and guanidine hydrochloride denaturation curves, *Methods Enzymol. 131*, 266−280.
18. Wüthrich, K. (1986) *NMR of proteins and nucleic acids*, Wiley, New York.
19. Christova, P., Cox, J. A., and Craescu, C. T. (2000) Ion-induced conformational and stability changes in *Nereis* sarcoplasmic calcium binding protein: evidence that the apo state is a molten globule, *Proteins*: *Struct., Funct., Genet. 40*, 177−184.
20. Barbato, G., Ikura, M., Kay, L. E., Pastor, R. W., and Bax, A. (1992) Backbone dynamics of calmodulin studied by ^{15}N relaxation using inverse detected two-dimensional NMR spectroscopy: the central helix is flexible, *Biochemistry 31*, 5269−5278.
21. Mercier, P., Li, M. X., and Sykes, B. D. (2000) Role of the structural domain of troponin C in muscle regulation: NMR studies of Ca^{2+} binding and subsequent interactions with regions 1−40 and 96−115 of troponin I, *Biochemistry 39*, 2902−2911.
22. Théret, I., Baladi, S., Cox, J. A., Sakamoto, H., and Craescu, C. T. (2000) Sequential calcium binding to the regulatory domain of Calcium Vector Protein reveals functional asymmetry and is accompanied by large structural changes, *Biochemistry 39*, 7920−7926.
23. Prêcheur, B., Cox, J. A., Petrova, T., Mispelter, J., and Craescu, C. T. (1996) *Nereis* sarcoplasmic Ca^{2+}-binding protein has a highly unstructured apo state which is switched to the native state upon binding of the first Ca^{2+} ion, *FEBS Lett. 395*, 89−94.
24. Théret, I., Baladi, S., Cox, J. A., Gallay, J., Sakamoto, H., and Craescu, C. T. (2001) Solution structure and backbone dynamics of the defunct domain of Calcium Vector Protein, *Biochemistry 40*, 13888−13897.
25. McPhalen, C. A., Strynadka, N. C. J., and James, M. N. G. (1991) Calcium-binding sites in proteins: a structural perspective, *Adv. Protein Chem. 42*, 77−144.
26. Biekovsky, R. R., Martin, S. R., Browne, J. P., Bayley, P. M., Feeney, J. (1998) Ca^{2+} coordination to backbone carbonyl oxygen atoms in calmodulin and other EF-hand proteins: ^{15}N chemical shifts as probes for monitoring individual-site Ca^{2+} coordination, *Biochemistry 37*, 7617−7629.
27. Zhang, M., Tanaka, T., and Ikura, M. (1995) Calcium-induced conformational transition revealed by the solution structure of apo calmodulin, *Nature Struct. Biol. 2*, 758−767.
28. Laskowski, R. A., Rullmann, J., Antoon, C., MacArthur, M. W., Kaptein, R., and Thornton, J. M. (1996) AQUA and PROCHECK-NMR: Programs for checking the quality of protein structures solved by NMR, *J. Biomolec. NMR 8*, 477−486.
29. Yap, K. L., Ames, J. B., Swindells, M. B., and Ikura, M. (1999) Diversity of conformational states and changes within the EF-hand protein superfamily, *Proteins: Struct., Funct., Genet. 37*, 499−507.
30. Babu, Y. S., Bugg, C. E., and Cook, W. J. (1988) Structure of calmodulin refined at 2.2 Å resolution, *J. Mol. Biol. 204*, 191−204.
31. Atkinson, R. A., Joseph, C., Kelly, G., Muskett, F. W., Frenkiel, T. A., Nietlisspach, D., and Pastore, A. (2001) Ca^{2+}-independent binding of an EF-hand domain to a novel motif in the α-actinin-titin complex, *Nature Struct. Biol. 8*, 853−857.
32. Ikura, M., Clore, G. M., Gronenborn, A. M., Zhu, G., Klee, C. B., and Bax, A. (1992) Solution structure of a calmodulin-target peptide complex by multidimensional NMR, *Science 256*, 632−638.
33. Meador, W. E., Means, A. R., and Quiocho, F. A. (1992) Target enzyme recognition by calmodulin: 2.4 Å structure of a calmodulin−peptide complex, *Science 257*, 1251−1255.
34. Meador, W. E., Means, A. R., and Quiocho, F. A. (1993) Modulation of calmodulin plasticity in molecular recognition on the basis of X-ray structures, *Science 262*, 1718−1721.
35. Osawa, M., Tokumitsu, H., Swindells, M. B., Kurihara, H., Orita, M., Shibanuma, T., Furuya, T., and Ikura, M. (1999) A novel

target recognition revealed by calmodulin in complex with Ca^{2+}-calmodulin-dependent kinase kinase, *Nature Struct. Biol. 6*, 819−824.
36. O'Neil, K. T., and DeGrado, W., F. (1990) How calmodulin binds its targets: sequence independent recognition of amphiphilic α-helices, *Trends Biochem. Sci. 15*, 59−64.
37. Rhoads, A. R., and Friedberg, F. (1997) Sequence motifs for calmodulin recognition, *FASEB J. 11*, 331−340.
38. Yap, K. L., Kim, J., Truong, K., Sherman, M., Youan, T., and Ikura, M. (2001) Calmodulin target database, *J. Struct. Funct. Genomics 1*, 8−14.
39. Clore, G. M., Bax, A., Ikura, M., and Gronenborn, A. M. (1993) Structure of calmodulin-target peptide complexes, *Curr. Opin. Struct. Biol. 3*, 838−845.
40. Martin, S. R., Bayley, P. M., Brown, S. E., Porumb, T., Zhang, M., and Ikura, M. (1996) Spectroscopic characterization of a high-affinity calmodulin−target peptide hybrid molecule, *Biochemistry 35*, 3508−3517.
41. Masino, L., Martin, S. R., and Bayley, P. M. (2000) Ligand binding and thermodynamic stability of a multidomain protein, calmodulin, *Protein Sci. 9*, 1519−1529.
42. Tsalkova, T. N., and Privalov, P. L. (1985) Thermodynamic study of domain organization in troponin C and calmodulin, *J. Mol. Biol. 181*, 533−544.
43. Comte, M., Maulet, Y., and Cox, J. A. (1983) Ca^{2+}-dependent high-affinity complex formation between calmodulin and melittin, *Biochem. J. 209*, 269−272.
44. Nicholls, A., Sharp, K. A., and Honig, B. (1991) Protein folding and association: insights from the interfacial and thermodynamic properties of hydrocarbons, *Proteins*: *Struct., Funct., Genet. 11*, 281−296.

BI0269714